Pure and Applied Geophysics

Marshall Islands Fringing Reef and Atoll Lagoon Observations of the Tohoku Tsunami

Murray Ford,[1] Janet M. Becker,[2] Mark A. Merrifield,[3] and Y. Tony Song[4]

Abstract—The magnitude 9.0 Tohoku earthquake on 11 March 2011 generated a tsunami which caused significant impacts throughout the Pacific Ocean. A description of the tsunami within the lagoons and on the surrounding fringing reefs of two mid-ocean atoll islands is presented using bottom pressure observations from the Majuro and Kwajalein atolls in the Marshall Islands, supplemented by tide gauge data in the lagoons and by numerical model simulations in the deep ocean. Although the initial wave arrival was not captured by the pressure sensors, subsequent oscillations on the reef face resemble the deep ocean tsunami signal simulated by two numerical models, suggesting that the tsunami amplitudes over the atoll outer reefs are similar to that in deep water. In contrast, tsunami oscillations in the lagoon are more energetic and long lasting than observed on the reefs or modelled in the deep ocean. The tsunami energy in the Majuro lagoon exhibits persistent peaks in the 30 and 60 min period bands that suggest the excitation of closed and open basin normal modes, while energy in the Kwajalein lagoon spans a broader range of frequencies with weaker, multiple peaks than observed at Majuro, which may be associated with the tsunami behavior within the more irregular geometry of the Kwajalein lagoon. The propagation of the tsunami across the reef flats is shown to be tidally dependent, with amplitudes increasing/decreasing shoreward at high/low tide. The impact of the tsunami on the Marshall Islands was reduced due to the coincidence of peak wave amplitudes with low tide; however, the observed wave amplitudes, particularly in the atoll lagoon, would have led to inundation at different tidal phases.

Key words: 2011 Tohoku tsunami, tide gauge records, Marshall Islands, coral reef, atoll.

1. Introduction

The magnitude 9.0 earthquake centered off the coast of Sendai, Japan (38.297°N, 142.372°E) on 11 March 2011 at 05:46:24 UTC triggered a tsunami with a highest recorded runup of 38.9 m, impacting much of the east coast of Honshu (Mori *et al.* 2011). The tsunami propagated across the Pacific Ocean (Fig. 1) with damage reported in Hawaii (Yamazaki *et al.* 2012), along the west coast of North America (Allan *et al.* 2012; Wilson *et al.* 2012), New Zealand (Borrero *et al.* 2012) and within parts of South America [National Geophysical Data Center/(NGDC/ WDS) Global Historical Tsunami Database, Boulder, CO, USA (Available at http://www.ngdc.noaa.gov/ hazard/tsu_db.shtml) 2011]. The impacts at Pacific Ocean atolls were relatively minor with no reports of significant injuries or damage, although wave over-topping at Midway Atoll in the Northwestern Hawaiian Islands resulted in the deaths of thousands of seabirds (US Fish and Wildlife Service 2011).

Historically, mid-ocean atolls have been vulnerable to coastal flooding and overwash during tsunami events. The 26 December 2004 magnitude 9.1 earthquake off the west coast of Sumatra generated a destructive tsunami which impacted numerous atolls in the Indian Ocean (Merrifield *et al.* 2005; Rabinovich and Thomson 2007). The Maldives, an atoll nation in the central Indian Ocean, was heavily impacted with an estimated death toll of 108 and US $295 million damage (NGDC/WDS). Tide gauge measurements of the Sumatran tsunami within the Maldives indicate maximum trough-to-crest wave heights of 2.15 and 2.17 m at Male and Hanimaadhoo atolls (Rabinovich and Thomson 2007). Geomorphic investigations showed that the tsunami was high enough to wash over many low-lying islands, depositing significant volumes of sand and gravel to

[1] School of Environment, The University of Auckland, Private Bag 92019, Auckland 1142, New Zealand. E-mail: m.ford@auckland.ac.nz
[2] Department of Geology and Geophysics, The University of Hawaii at Manoa, Honolulu, HI 96822, USA.
[3] Department of Oceanography, The University of Hawaii at Manoa, Honolulu, HI 96822, USA.
[4] Jet Propulsion Laboratory, California Institute of Technology, Pasadena, CA 91109, USA.

the islands (KENCH et al. 2006). The highest tsunami-associated water level recorded by a tide gauge on a Pacific atoll was 1.90 m at Midway atoll following the magnitude 8.2 Kamchatka earthquake in 1952 (NGDC/WDS). A tide gauge operating since 1946 on Kwajalein Atoll (8.732°N, 167.735°E) recorded 26 unique tsunami events prior to the Tohoku tsunami, the highest of which was 0.38 m (NGDC/WDS).

Local topographic effects on tsunamis have been noted at mid-ocean atolls. VAN DORN (1984) summarized attempts to account for the modification of a mid-ocean tsunami by Wake Island, and noted the excitation of high frequency oscillations (31 cph) in tide gauge records located within a small boat harbor. HEIDARZADEH and SATAKE (2013) characterized the Tohoku tsunami at the Kwajalein and Wake atolls based on tide gauge records, and noted a broad frequency response in the first hour of arrival followed by more narrow-banded oscillations at both sites. In general, tide gauge observations of tsunamis at atolls and island stations tend to show a more rapid decay than stations along continental margins (MERRIFIELD et al. 2005; HEIDARZADEH and SATAKE 2013), likely due to the lack of well-defined shelves at most islands (HEIDARZADEH and SATAKE 2013). Atolls encompass a range of topographically complex sub-environments within enclosed or semi-enclosed lagoons and along ocean-facing reefs at the atoll rim. Typically a single lagoon tide gauge record may be available, with few direct observations to assess the response in the various atoll sub-regions.

Fringing coral reefs are highly efficient attenuators of wind wave energy (e.g. LUGO-FERNÁNDEZ et al. 1998; PEQUIGNET et al. 2011), affording the protection necessary for human occupation of low-lying reef islands. Impact assessments following the 2004 Sumatran tsunami found no clear association between the presence of coral reefs and reduced runup and inundation (ADGER et al. 2005; BAIRD et al. 2005; GOFF et al. 2006). In an analysis of 62 sites impacted by the Sumatran tsunami, CHATENOUX and PEDUZZI (2007) noted a positive relationship between the presence of a coral reef and the extent of inundation. We find few applications of numerical models of tsunami propagation within reef settings (KUNKEL et al. 2006; LYNETT 2007; GELFENBAUM et al. 2011) and none within mid-ocean atoll settings. In a

numerical study of tsunami propagation around an idealised circular island KUNKEL (2006) found that wide, shallow lagoons were effective at reducing tsunami impact. Similarly, in a detailed numerical study of tsunami propagation across fringing coral reefs GELFENBAUM et al. (2011) found that wide and rough reef flats provide the greatest attenuation of tsunami energy. However, GELFENBAUM et al. (2011) report shoaling of tsunami exceeded dissipation on narrow reefs (<200 m) resulting in higher amplitudes at the shoreline than incident at the reef edge.

Here we describe high-frequency water level measurements of the 2011 Tohoku tsunami recorded within a range of environments on two mid-ocean atolls in the Marshall Islands (Fig. 1). Sixteen pressure gauges and two permanent tide gauges at Kwajalein and Majuro atolls provide concurrent measurements of tsunami waves in the inner and outer waters of a mid-ocean atoll. The atoll water level observations are complemented by information of the tsunami in deep-water from pressure measurements at a nearby Deep-Ocean Assessment and Reporting of Tsunamis (DART) buoy and from numerical model simulations of the event (Fig. 1). The observations provide the first high-frequency
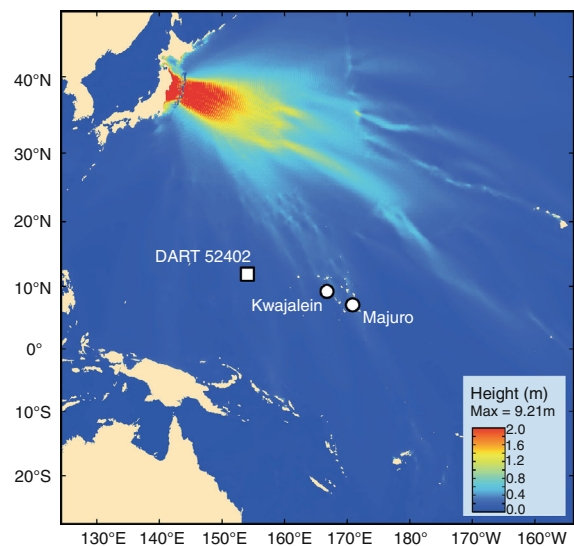

Figure 1
Modelled maximum predicted height of the Tohoku tsunami (SONG 2012), DART buoy #52402 and study sites within the Marshall Islands

record of tsunami propagation throughout a reef/atoll setting and afford a unique opportunity to assess the tsunami response at different geomorphic locations throughout an atoll. In addition, the study provides further context of the tsunami signal detected by atoll lagoon tide gauges, which are an important component of Pacific and Indian Ocean tsunami warning networks.

2. Description of Measurements and Model Output

As part of a study to investigate wind wave processes on fringing coral reefs, bottom mounted pressure sensors were deployed within the lagoon and on the ocean-facing fringing reef at Majuro and Kwajalein atolls within the Republic of the Marshall Islands (Fig. 2). Instruments at Majuro were
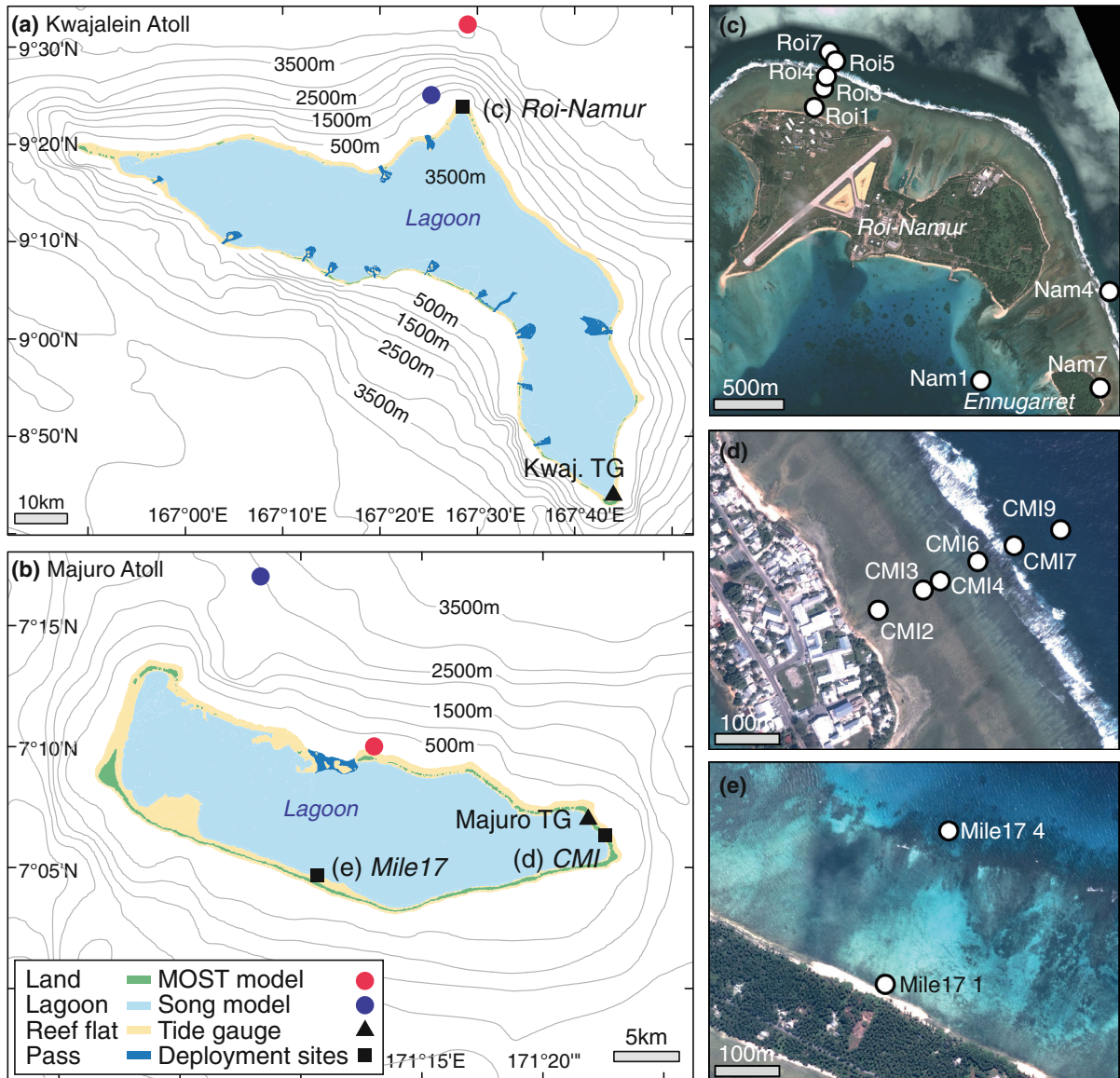

Figure 2

Locations of numerical simulation of tsunami propagation, tide gauge and deployment sites on Kwajalein (**a**) and Majuro (**b**) atolls. Pressure sensor locations at Roi-Namur (**c**), College of the Marshall Islands (CMI) (**d**) and Mile 17 (**e**). Imagery copyright DigitalGlobe, all rights reserved
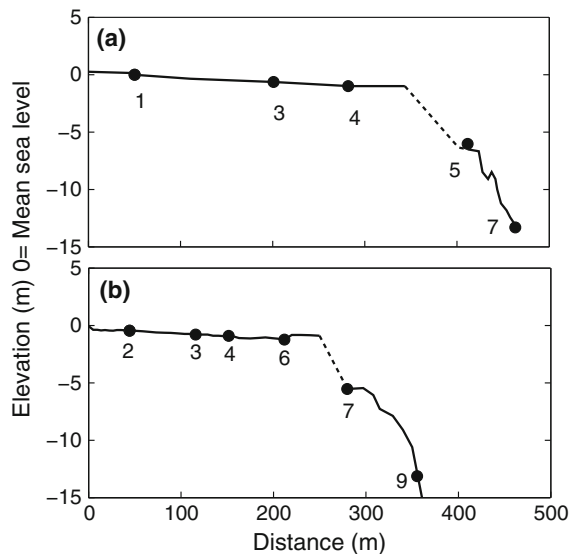
Figure 3
Cross-reef bathymetry at Roi (**a**) and CMI (**b**) showing instrument locations

Table 1

Instrument type and sampling scheme for the pressure data used in this analysis

Instrument	Type	Sampling	Depth (m)
Roi 7	AWAC	0.21/1 h	13.8
Roi 5	SeaBird	1.5/3 h	6.2
Roi 4	Aquadopp	1.5/3 h	0.8
Roi 3	SeaBird	1.5/3 h	0.7
Roi 1	SeaBird	1.5/3 h	0.4
Nam 4	SeaBird	1.5/3 h	7.7
Nam 7	SeaBird	1.5/3 h	0.4
Nam 1	SeaBird	1.5/3 h	3.1
CMI 9	AWAC	0.21/1 h	13.8
CMI 7	SeaBird	1.5/3 h	5.3
CMI 6	Aquadopp	1.5/3 h	1.0
CMI 4	SeaBird	1.5/3 h	0.8
CMI 3	Aquadopp	1.5/3 h	0.8
CMI 2	SeaBird	1.5/3 h	0.5
Mile 17 4	SeaBird	0.33/1 h (2 Hz)	5.1
Mile 17 1	SeaBird	0.33/1 h (2 Hz)	0.9

All instruments sampled at 1 s unless indicated. "AWAC" indicates the Nortek Acoustic Wave and Current Profiler, "Seabird" the Seabird SBE26 plus Wave and Tide Record, and "Aquadopp" the Nortek Aquadopp acoustic Doppler current meter. Sampling indicates the duration of the burst sample/interval between burst samples

deployed on the reef adjacent to the College of the Marshall Islands (CMI, Figs. 2b, d, 3) and within the lagoon at a site known locally as Mile 17 (Fig. 2b, e). Instruments at Kwajalein were deployed at Roi-Namur, two islands connected by reclaimed land at the north of Kwajalein atoll (Fig. 2a, c). Five instruments were deployed along a shore perpendicular transect extending from the shoreline at Roi (Fig. 3). At Namur instruments were deployed across the reef flat between Namur and Ennugarret Island, including instruments at the toe of beach at Ennugarret Island (Nam7) (Fig. 2c). The fringing reef flats at each site are near-horizontal, intertidal surfaces with steep (5°–8°) reef faces (Fig. 3).

The pressure sensors were configured and deployed to investigate wind waves (periods of 3–30 s), infragravity waves (30–600 s), and breaking wave setup on the shallow reef flats. As such, 1-s samples over 1.5 h records every 3 h were collected. Instrument descriptions and sampling schemes are presented in Table 1. Infragravity waves have complicated the detection of tsunami signals within nearshore records and are typically low-pass filtered prior to analysis to isolate the tsunami signal (RABINOVICH et al. 2006, 2011). While infragravity waves at Kwajalein and Majuro have been observed with periods exceeding 6 min during large swell events in

the complete data set, the moderate incident wave heights during the tsunami suggest that the observed low frequency energy may be attributed to the tsunami. As a result, the predicted tide was removed from each pressure time series and a low-pass filter was applied with a cut-off period of 6 min. For the Mile 17 pressure time series in the Majuro lagoon, a 30 s cut-off period was used due to the reduced wind-wave and infragravity energy compared to the outer reef. Surface elevation is computed from bottom pressure assuming a hydrostatic balance.

Tide gauge records were obtained from the US Army Kwajalein Airbase within the lagoon at the southern end of Kwajalein Atoll (1 min averages) and at Uliga dock, on the lagoon shoreline in the east of Majuro Atoll (6 min averages). The tide gauges sampled continuously throughout the event with the exception of a 24 min gap in the Kwajalein record (at 10:23 in Fig. 4a). Time series from the nearest DART buoy that was operational during the tsunami (buoy 52402) provides deep water measurements (1 min averages) of the tsunami wave approximately 1,500 km WNW of Kwajalein (Fig. 1).
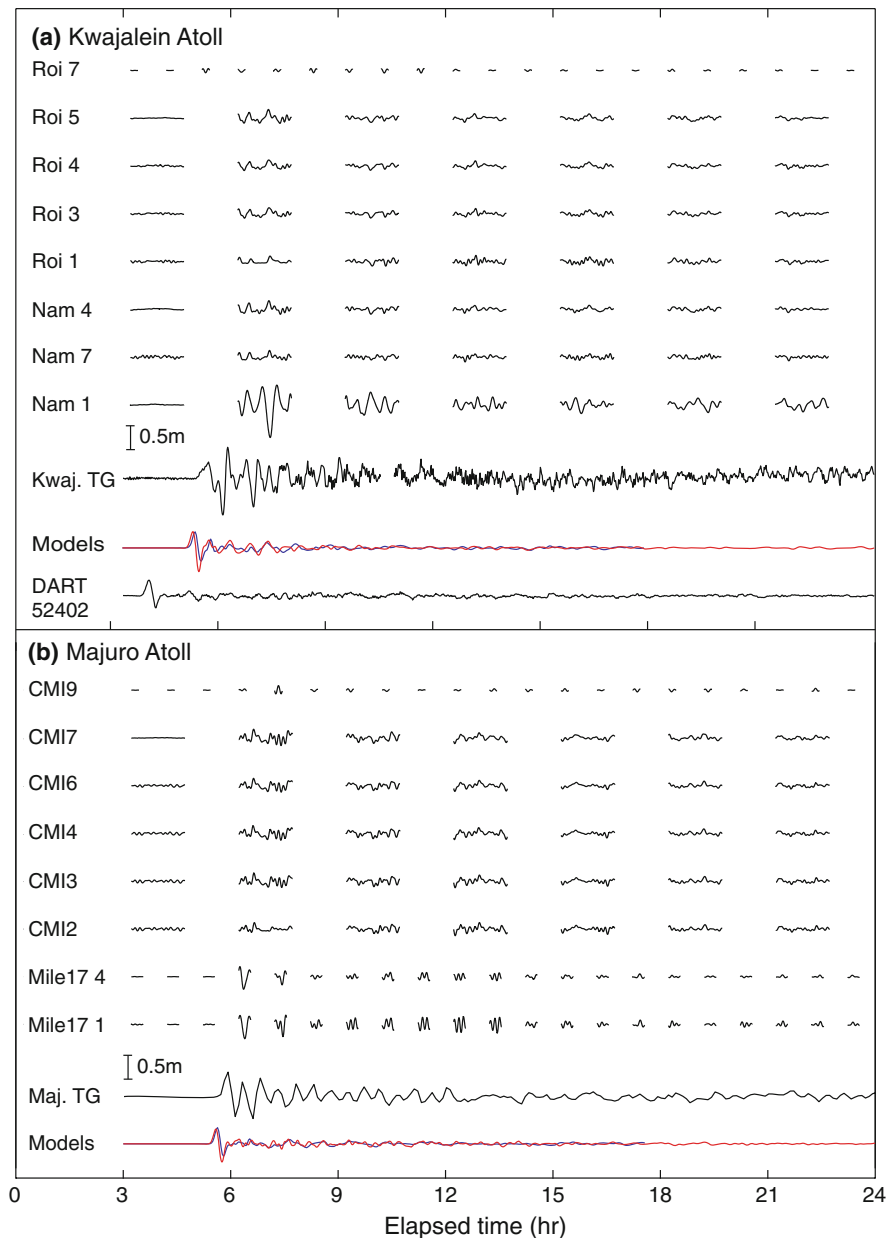
Figure 4

a De-tided surface elevation time series showing tsunami waves at **a** Kwajalein Atoll, and **b** Majuro Atoll. The model results are from deep water grid points near the respective atolls (*red line* = MOST, *blue line* = Song) (Fig. 2)

As a result of the significant distance between both Kwajalein and Majuro atolls and the DART buoy, outputs of two previously published tsunami propagation models are presented to provide deep water estimates of tsunami amplitude close to each atoll rim. The numerical models are referred to as the Song model (SONG *et al.* 2012) and the MOST model

(TITOV and GONZALEZ 1997). The Song tsunami model is a simplified version of the three-dimensional ocean circulation model of SONG and HOU (2006). The tsunami is generated by the earthquake-induced seafloor motions, as formulated in SONG *et al.* (2008). The model grid is configured to cover the entire Pacific Ocean with a 1/12° horizontal resolution and 30

terrain-following vertical levels. The time step is 3 s and the results are saved every 40 steps. Similarly, outputs of the MOST model cover the Pacific Ocean and are stored spatially at 16 arcmin with a 60 s time step (TANG et al. 2012). Time series were extracted from both models at the closest model points northwest of each atoll (Fig. 2). The Marshall Islands and the DART buoy are located south of the main beam of tsunami energy radiating from the source region in the model simulations (Fig. 1).

3. Observations of the Tohoku Tsunami in the Marshall Islands

The Kwajalein and Majuro tide gauge records indicate a leading positive elevation wave at 10:51 and 11:24 UTC respectively (or 05:06 and 05:39 elapsed time in Fig. 4a, b), with the first crest highest at Majuro (0.50 m) and the second crest highest at Kwajalein (0.61 m). Applying a 6 min running mean filter to the Kwajalein record, to match the Majuro record, reduced the peak amplitude to 0.45 m. The 1-min sampling at Kwajalein shows an initial minima following the first crest, and then a substantial trough of −0.81 m. The initial wave height at Kwajalein is, therefore, somewhat uncertain, but the height measured from the crest to the larger trough corresponds to 1.42 m. The initial crest-to-trough wave height at the Majuro tide gauge is 0.93 m, which is greater than the height measured and estimated in the deep ocean, with the DART buoy and the models showing a prominent initial crest-to-trough height of 0.58–0.69 m (Fig. 4a, b).

Most of the Roi-Namur and Majuro pressure sensors began a burst record at 12:00 UTC, which missed the initial wave arrival but captured the wave form soon after the second crest as indicated by the tide gauge records (Fig. 4a, b). The water level oscillations in the lagoons (Nam1, Mile17) resemble those captured by the tide gauges, with a peak amplitude at Nam1 of 0.41 m. The tsunami amplitudes on the ocean-facing fringing reefs at both study sites are significantly weaker than in the lagoons (Fig. 4). The maximum recorded water level amplitudes are 0.18 m on the reef faces (Nam4, Roi5, CMI7), reducing to 0.13–0.14 m on the reef flats. During the same burst sample records, the peak amplitudes in the lagoons are 0.35 and 0.38 m at the Kwajalein and Majuro tide gauges respectively.

Wave model simulations of the tsunami elevation at grid points in deep water (Fig. 2) compare favorably with the reef face pressure time series at Majuro and Kwajalein (CMI7, Roi5, Nam4) during the first two measured sampling bursts, low-pass filtered with a cut-off period of 6 min (Fig. 5). We emphasize that the model time series and the reef face observations are not sampled at the same location. The agreement is better during the more energetic initial burst, and in general the MOST model matches the observations more closely than the Song model, although both models provide a reasonable approximation of the observations. The first wave of elevation was not measured on the reef flats; however, if the first waves scale with the deep water signal in a similar manner as shown in Fig. 5, then we would estimate the first wave arrival to be ∼0.3 m in amplitude. When added to the tidal level, this would lead to a total water level that is ∼0.5 m below the previous high tide and >1 m below maximum spring tide levels. The relatively low total water level is consistent with the lack of coastal inundation reported during the tsunami on the outer shores of both atolls.

Hours after the initial wave arrival, the tsunami energy on the outer reefs is less energetic than in the atoll lagoons, but more energetic than in the deep ocean as indicated by the models or the DART buoy observations. We note that cross-shore standing mode periods for the shallow reef flats are on the order of minutes, compared to the much longer periods of modal oscillations in the deeper, broader atoll lagoons (see Sect. 4). The spectral characteristics of the deep water tsunami are discussed in Sect. 4 below. Deep-water properties of the Tohoku tsunami also have been discussed by HEIDARZADEH and SATAKE (2013), BORRERO and GREER (2013), RABINOVICH et al. (2013) and others.

Instruments in the Majuro lagoon at Mile 17 were deployed across a shallow subtidal reef, with Mile17 1 located near the toe of the island beach and Mile17 4 in ∼5.1 m depth. During the first post-arrival burst sample, 20 min water level records at Mile17 show similar wave forms at the shallow
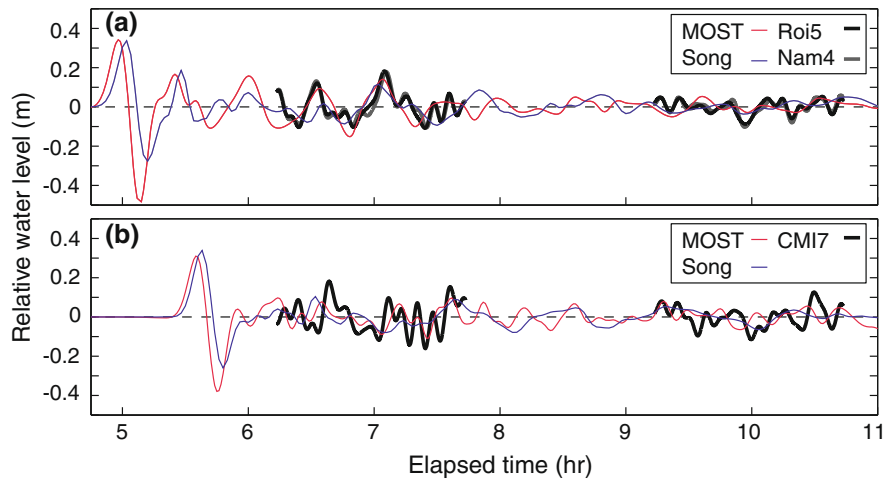
Figure 5
Surface elevation time series showing tsunami waves on the reef face at Kwajalein Atoll (**a**, **b**), and Majuro Atoll (**c**). The model results are from deep water grid points shown in Fig. 2

and deep sensors, with amplitudes of 0.31 and 0.29 m at Mile17 1 and Mile17 4, respectively (Fig. 6a). Phase and amplitude differences between the two locations begin to appear in the next sample (Fig. 6b). During subsequent bursts, the deep and shallow oscillations are approximately 180° out of phase, the dominant period falls below 6 min, and the maximum amplitudes at the shoreline are between 0.05 and 0.17 m higher than at 5.1 m depth (Fig. 6c–e). The high frequency behavior suggests the presence of edge waves in the lagoon, that would not be well captured in the Majuro tide gauge record, with a 6 min sample period.

On the outer fringing reefs, the effects of tidal level on tsunami propagation across the reef flats is evident (Fig. 7). Focussing on the first post-arrival burst sample measured by the pressure sensors at Roi, we see that wave crests propagate on to the reef flat at low tide. Cross-reef time lags and amplitude decay are observed as the wave crests separated by 20–30 min propagate over the tidally exposed reef flat (Fig. 7a). The low water level causes slow wave speeds and enhanced dissipation. In contrast, at high tide (Fig. 7b), wave crests and troughs are observed on the reef, the time lags are short between sensors, and short period (<30 min) wave amplitudes increase toward shore, presumably due to enhanced shoaling relative to dissipation with higher water levels over the reef flat than at low tide.

4. Tide Gauge and Lagoon Oscillations

As is evident from Fig. 4, the lagoon response to the tsunami is amplified compared to the outer reefs of the two atolls. To characterize the spectral character of the tsunami in the atoll lagoons further, a wavelet analysis of the continuous tide gauge records is performed (Fig. 8). We use a Morlet wavelet following the procedures described by TORRENCE and COMPO (1998). The 24-min gap in the Kwajalein time series is filled with linear interpolation and all time series have the predicted tide removed and are high-passed filtered (8-h cut-off period). The wavelet spectra are normalized by the variance at each station and plotted in Fig. 8 as decibels below the peak value.

As discussed by HEIDARZADEH and SATAKE (2013), the tsunami signal at Kwajalein initially (first 2 h after arrival) exhibits energy over a broad range of periods, 15–80 min with a peak ~30 min, followed by sustained energy in the 30–80 min period range (Fig. 8a). In contrast, Majuro shows energy in two prominent bands, 20–40 min and 50–80 min, with peak periods of ~30 and 70 min (Fig. 8b). Ringing in these bands persists for days at Majuro, particularly in the 20–40 min band. A notable energy maxima approximately 40–50 h after the tsunami event likely represents the arrival of reflected wave energy, as noted by HEIDARZADEH and SATAKE (2013).
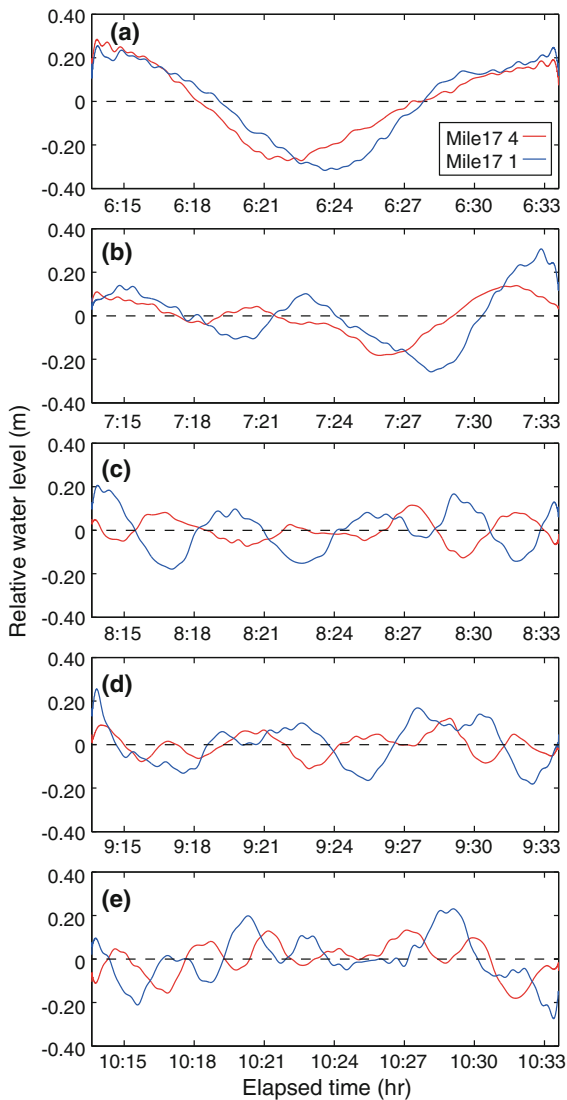
Figure 6
Spectrally filtered (30 s cut-off) water level records from Mile 17 during the first five post-tsunami bursts
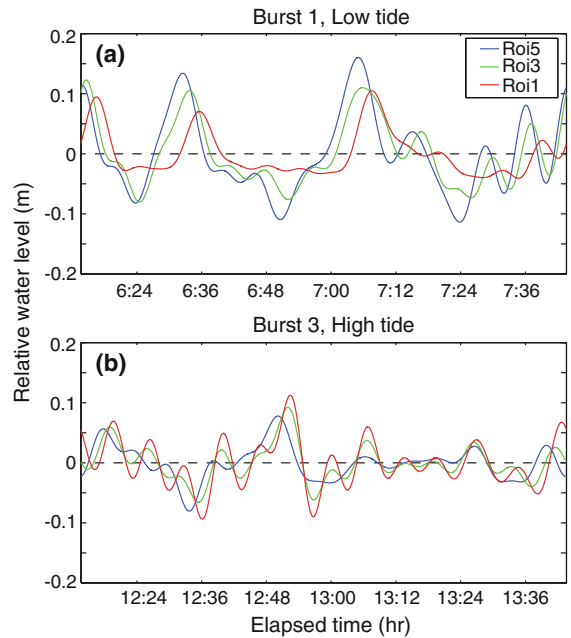

Figure 7
Effects of tidal level on tsunami propagation across the reef at Roi. The *top panel* shows the decay in amplitude and propagation speed of the first measured burst of the tsunami across the reef at low tide. The *bottom panel* shows an increase in the amplitude of the tsunami shoreward during high tide as measured in burst 3. The location of sensors are indicated in the *legend*

We next use autospectra to characterize the frequency content of the tsunami signals at each tide gauge in comparison to deep ocean estimates from the model simulations. Based on the wavelet results (Fig. 8), we focus on the 15-h time span following the initial arrival of the tsunami. At the Kwajalein tide gauge, the tsunami energy is broad-banded with four spectral peaks that are just barely significant at the 95 % level (Fig. 9a). In the deep ocean, the models show energy over a similar broad band without noted spectral peaks, except for the MOST model,

which indicates prominent deep ocean energy near 30 min period. The difference in lagoon and deep ocean spectra is even more pronounced at Majuro, where the two spectral peaks seen in the wavelet spectra (Fig. 8b) are prominent in the tide gauge autospectrum (Fig. 9b), and both peaks are absent in the deep ocean model spectra. It appears that the tsunami generates basin modes specific to each lagoon.

We further describe the spectral properties of the tsunami from the lagoon tide gauge records following RABINOVICH *et al.* (2013). In Fig. 10, we compare the background spectra (S_b) calculated from the tide gauge records for ~10.5 days prior to the onset of the tsunami, to that estimated from the tide gauge records for 15 h during the tsunami (S_t). The background spectra have been smoothed over 112 frequency bands and the tsunami spectra over seven frequency bands. For the Kwajalein background spectral estimates, gaps ranging from 2 to 19 min were filled using linear interpolation. While the
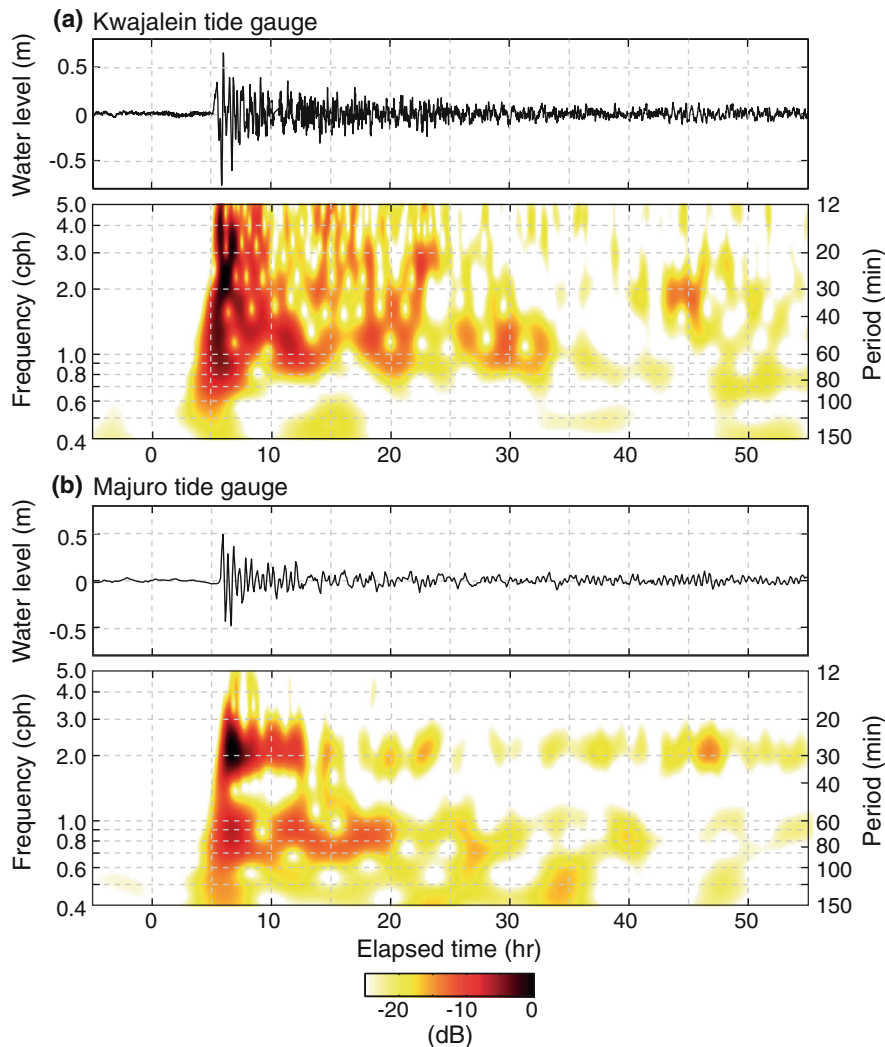
Figure 8
Time series and wave spectra for the **a** Kwajalein and **b** Majuro tide gauge records. Elapsed time is referenced to the start of the Tohoku tsunami event at 3/11/2011 5:46:24 UTC. The wavelet spectra are computed after removing the predicted tide and high-pass filtering (8-h cut-off period) the time series. The spectra are normalized by the variance of each time series, and the contour plots are presented in decibels (dB) below the maximum value of each spectral plot

Majuro tide gauge record was continuous, the 6-min sample period set the high frequency cut-off for the Majuro spectral estimates. At both locations, S_b and S_t exhibit similar energy levels at periods <150 min (Fig. 10a, b). Energy during the tsunami also is higher than the background at Kwajalein out to the highest frequencies measured, which agrees with the high frequency energy observed in the Majuro lagoon pressure records. The ratio of the spectra during the tsunami to the background, S_t/S_b, is used to minimize the effects of the local topography (RABINOVICH et al.

2013). The broad spectral peak between the 20 and 60 min period is fairly consistent at the two sites when correcting for the background spectra (Fig. 10c). The distinct spectral peaks at each site are well above background levels. The Marshall Islands spectral ratios (Fig. 10c) also resemble ratios obtained from an average of all available open-ocean DART records (RABINOVICH et al. 2013) and from tide gauge records along the Pacific coast of Russia (SHEVCHENKO et al. 2014). The spectral character of the Tohoku tsunami, normalized by background
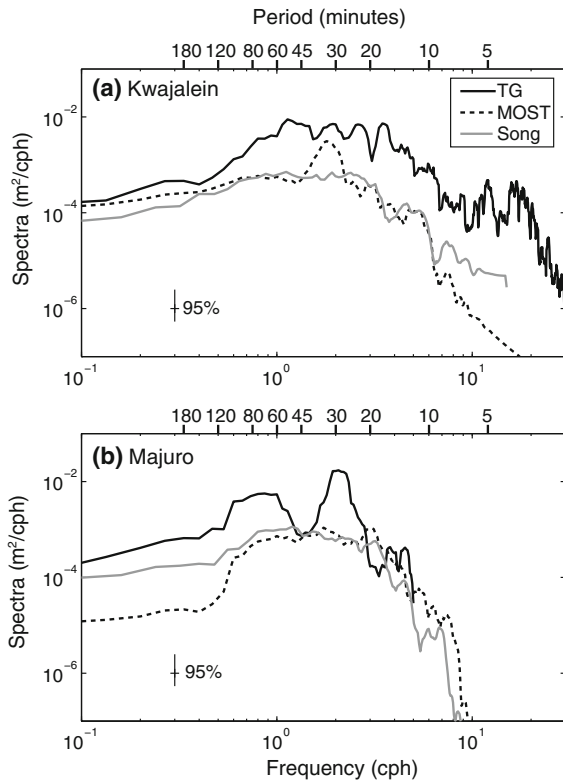
Figure 9
Autospectra of water level from the tide gauge observations (TG), MOST model output (MOST), and Song model output (Song) for **a** Kwajalein and **b** Majuro. Spectra are computed for the time period 3/11/2011 10:49 UTC to 3/12/2011 1:49. The predicted tide has been removed from the TG time series. 95 % confidence intervals are obtained by smoothing over 7 adjacent frequencies

Figure 10
Autospectra computed before, S_b (3/1/2011 0:00 UTC to 3/11/2011 10:49), and after, S_t (3/11/2011 10:49 to 3/12/2011 1:49), the arrival of tsunami waves observed at the **a** Kwajalein and **b** Majuro tide gauges. 95 % confidence intervals are computed based on the S_t estimate obtained by smoothing over seven adjacent frequencies. **c** The ratio S_t/S_b for the Kwajalein and Majuro tide gauges

spectra, appears to have been remarkably consistent, even at sites well north (Russia) and south (Marshall Islands) of the main beam of wave energy.

The presence of spectral peaks and persistent "ringing" of the tsunami signal at the Majuro atoll lagoon suggests that natural modes of oscillation have been excited by the deep water tsunami, with dominant periods illustrated in Figs. 8, 9, 10. At Majuro, the observed spectral peaks agree with qualitative estimates of the dominant modal periods. Treating the Majuro lagoon as rectangular in shape ($L = 37$ km, $W = 8$ km) and predominantly enclosed with an average depth of $h = 40$ m, we estimate that the period of a one-dimensional 1/2 wavelength mode at Majuro is $2L(gh)^{-1/2} = 62$ min, and 1 wavelength mode is $L(gh)^{-1/2} = 31$ min, roughly matching periods of the observed spectral peaks. While the
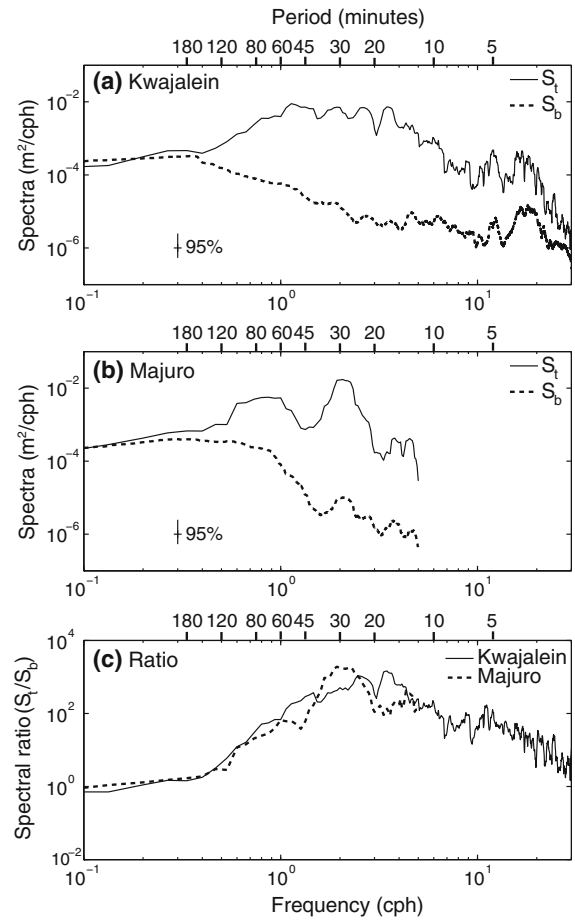
Majuro lagoon is predominantly enclosed, with a dry or shallow water reef enclosing most of the lagoon, one ~3.5 km wide pass exists on the north-facing rim of the atoll and a narrow, artificial boat channel is found on the southern rim. Hence, the possibility exists that a 1/4 wavelength mode in width, $4 W(gh)^{-1/2}$, may be excited in the lagoon. For Majuro, the period of the 1/4 wavelength mode is 27 min. Comparing the tide gauge time series with the pressure records at Mile17 indicates an approximate 180° phase shift between the sites, which appears to favor the one-wavelength (closed basin)

major axis mode rather than the quarter-wavelength (open basin) minor axis mode. At Kwajalein, the complicated geometry of the lagoon precludes simple estimates of the closed and open basin normal modes. A more detailed model analysis using the actual bathymetry and boundary conditions is required to determine the character of the normal modes at both atolls, which at present is limited by the lack of high resolution topography.

5. Discussion and Implications for Atoll Islands

The amplitude of the Tohoku tsunami was the largest recorded at Kwajalein atoll since the tide gauge began operation in 1946. However, the Tohoku tsunami caused no reported inundation within the Marshall Islands. This is a fortuitous function of the initial and potentially highest amplitude motions coinciding with low-tide. The wave amplitude along the ocean-facing reef flat was considerably lower than within the lagoon, similar to deep ocean values, at least after the initial crest arrival. The initial peak of the tsunami was unrecorded by the fringing reef instruments. The total water level fluctuations recorded at all sites, including the tidal component, did not exceed the level of the preceding high tide. Although direct observations are lacking, we speculate that the same would hold for reef-protected shorelines around the perimeter of the atoll. Assuming that the amplitude of the initial crest on the reef flats scales with the modeled deep-ocean tsunami in a similar manner as observed for subsequent lower amplitude crests (Fig. 5), then we would expect the initial tsunami crest amplitudes on the reef flat to be lower than what was observed by the lagoon tide gauges.

Observations of tsunami behavior on the ocean-facing reef flats are broadly consistent with results of numerical models (GELFENBAUM et al. 2011). With the exception of the first post-tsunami burst, during which time the tsunami propagated across a dry reef flat and subsequent measurements at low tide, we find that the tsunami increases in height while propagating across the reef flat. GELFENBAUM et al. (2011) show that on narrow reef flats (<200 m) shoaling exceeds dissipation, driving higher shoreline runup levels. Reef flats at the Roi-Namur and CMI sites range between 240

and 350 m wide. Elsewhere in Kwajalein and Majuro ocean-facing reef flats range in width; in places, intertidal reef flats are narrower than 100 m. Similarly, the width and depth of sub- and intertidal reefs within the lagoon vary considerably, likely to result in considerable spatial variability in shoreline runup levels. At present, assessing potential tsunami-driven inundation, particularly at Majuro is problematic as no high-quality topographic datasets exist.

Atoll islands are particularly low-lying, with areas neighboring the lagoon typically the lowest coastal relief (WOODROFFE 2008). Relatively small positive sea level anomalies (<0.30 m) associated with ENSO cycles have been documented to drive inundation of lagoon-facing sections of Majuro during spring tides (FORD et al. 2012). As a result, a wave sharing similar characteristics as the Tohoku tsunami would have been high enough to exceed the topographic threshold had the peak coincided with higher tidal levels. Lagoon shorelines are typically sheltered from ocean swells and have lower levels of exposure to storm-driven inundation. Since WWII Majuro atoll has undergone rapid population growth and intensification of development (SPENNEMANN 1996). Significant key infrastructure including the airport, port and power station are located along the lagoon shore, along with dense housing, which occupies nearly all available land within the urban sections of Majuro.

Relative to storm-driven inundation, tsunamis have to date caused no documented impact in the Marshall Islands. However, the impact of the 2004 Sumatran tsunami in the Maldives does illustrate the potential for high impact tsunami events on atolls (NGDC/WDS). As a result, hazard mitigation and preparedness plans for atolls require careful consideration of the risks associated with tsunamis. Within atoll settings ocean-facing sections of the islands are most exposed to storm-associated hazards, particularly wave overwash. Our results show the likelihood that settings considered sheltered from storm-driven inundation, namely the inner lagoon shoreline, are not immune to inundation associated with the long-wave forcing caused by tsunamis, particularly if the resonant frequencies of the lagoon match energetic portions of the tsunami spectrum.

REFERENCES

ADGER, W.N., T.P. HUGHES, C. FOLKE, S.R. CARPENTER, and J. ROCKSTRÖM (2005). *Social-ecological resilience to coastal disasters*, Science, *309*, 1036–1039. doi:10.1126/science.1112122.

ALLAN, J.C., P.D. KOMAR, P. RUGGIERO, and R. WITTER (2012). *The March 2011 Tōhoku Tsunami and Its Impacts along the US West Coast,* J. Coast. Res. *28*, 1142–1153. doi:10.2112/JCOASTRES-D-11-00115.1.

BAIRD, A.H., S.J. CAMPBELL, A.W. ANGGORO, R.L. ARDIWIJAYA, N. FADLI, Y. HERDIANA, T. KARTAWIJAYA, D. MAHYIDDIN, A. MUKMININ, and S.T. PARDEDE (2005). *Acehnese reefs in the wake of the Asian tsunami,* Curr. Biol., *15*, 1926–1930. doi:10.1016/j.cub.2005.09.036.

BORRERO, J.C., BELL, R., CSATO, C., DELANGE, W., GORING, D., GREER, S.D., PICKETT, V. and POWER, W. (2012). *Observations, effects and real time assessment of the March 11, 2011 Tohoku-oki tsunami in New Zealand,* Pure and Appl. Geophys., *170*, 1229–1248. doi:10.1007/s00024-012-0492-6.

BORRERO, J.C. and S.D. GREER (2013). *Comparison of the 2010 Chile and 2011 Japan tsunamis in the far field*, Pure Appl. Geophys. *170*, 1249–1274. doi:10.1007/s00024-012-0559-4.

CHATENOUX, B. and P. PEDUZZI (2007). *Impacts from the 2004 Indian Ocean Tsunami: analysing the potential protecting role of environmental features*, Nat. Hazards, *40*, 289–304. doi:10.1007/s11069-006-0015-9.

FORD, M.R., J.M. BECKER, and M.A. MERRIFIELD (2012). *Spatial and temporal controls of atoll island inundation: implications for urbanized atolls in the Marshall Islands*. (Invited), 2012 AGU Fall Meeting.

GELFENBAUM, G., A. APOTSOS, A.W. STEVENS, and B. JAFFE (2011). *Effects of fringing reefs on tsunami inundation: American Samoa*, Earth-Sci. Rev., *107*, 12–22. doi:10.1016/j.earscirev.2010.12.005.

GOFF, J., P.L. LIU, B. HIGMAN, R. MORTON, B.E. JAFFE, H. FERNANDO, P. LYNETT, H. FRITZ, C. SYNOLAKIS, and S. FERNANDO (2006). *Sri Lanka field survey after the December 2004 Indian Ocean tsunami,* Earthquake Spectra, *22*, 155–172. doi:10.1193/1.2205897.

HEIDARZADEH, M. and K. SATAKE (2013). *Waveform and spectral analyses of the 2011 Japan tsunami records on tide gauge and DART stations across the Pacific Ocean*, Pure Appl. Geophys., *170*, 1275–1293. doi:10.1007/s00024-012-0558-5.

Kench, P.S., R.F. McLean, R.W. Brander, S.L. Nichol, S.G. Smithers, M.R. Ford, K.E. PARNELL, and M. ASLAM (2006). *Geological effects of tsunami on mid-ocean atoll islands: The Maldives before and after the Sumatran tsunami,* Geology, *34*, 177–180. doi:10.1130/G21907.1.

KUNKEL, C.M., R.W. HALLBERG, and M. OPPENHEIMER (2006). *Coral reefs reduce tsunami impact in model simulations,* Geophys. Res. Lett., *33*, L23612. doi:10.1029/2006GL027892.

LUGO-FERNÁNDEZ, A., H.H. ROBERTS, and J.N. SUHAYDA (1998). *Wave transformations across a Caribbean fringing-barrier coral reef,* Cont. Shelf Res., *18*, 1099–1124.

LYNETT, P.J. (2007). *Effect of a shallow water obstruction on long wave runup and overland flow velocity,* J. of Waterway, Port, Coastal, and Ocean Eng., *133*, 455–462. doi:10.1061/(ASCE)0733-950X(2007)133:6(455).

MERRIFIELD, M., Y. FIRING, T. AARUP, W. AGRICOLE, G. BRUNDRIT, D. CHANG-SENG, R. FARRE, B. KILONSKY, W. KNIGHT, and L. KONG (2005). *Tide gauge observations of the Indian Ocean tsunami, December 26, 2004,* Geophys. Res. Lett., *32*, L09603. doi:10.1029/2005GL022610.

MORI, N., T. TAKAHASHI, T. YASUDA, and H. YANAGISAWA (2011). *Survey of 2011 Tohoku earthquake tsunami inundation and run-up,* Geophys. Res. Lett., *38*, L00G14. doi:10.1029/2011GL049210.

NATIONAL GEOPHYSICAL DATA CENTER (NGDC) (2012). *March 11, 2011 Japan Earthquake and Tsunami.* http://www.ngdc.noaa.gov/hazard/honshu_11mar2011.shtml. Accessed 09/28/2013.

PÉQUIGNET, A., J. BECKER, M. MERRIFIELD, and S. BOC (2011). *The dissipation of wind wave energy across a fringing reef at Ipan, Guam,* Coral Reefs, *30*(1), 71–82. doi:10.1007/s00338-011-0719-5.

RABINOVICH, A.B., R.E. THOMSON, and F.E. STEPHENSON (2006). *The Sumatra tsunami of 26 December 2004 as observed in the North Pacific and North Atlantic oceans,* Surv. Geophys., *27*(6), 647–677. doi:10.1007/s10712-006-9000-9.

RABINOVICH, A.B. and R.E. THOMSON (2007). *The 26 December 2004 Sumatra tsunami: Analysis of tide gauge data from the world ocean Part 1. Indian Ocean and South Africa.* Pure Appl. Geophys. *164*, 261–308. doi:10.1007/s00024-006-0164-5.

RABINOVICH, A., K. STROKER, R. THOMSON, and E. DAVIS (2011). *DARTs and CORK in Cascadia Basin: High-resolution observations of the 2004 Sumatra tsunami in the northeast Pacific,* Geophys. Res. Lett., *38*(8), L08607. doi:10.1029/2011GL047026.

RABINOVICH, A.B., R.N. CANDELLA, and R.E. THOMSON (2013). *The open ocean energy decay of three recent trans-Pacific tsunamis,* Geophys. Res. Lett. *40*, 3157–3162. doi:10.1002/grl.50625.

SHEVCHENKO, G., T. IVELSKAYA, and A. LOSKUTOV (2014). *Characteristics of the 2011 Great Tohoku Tsunami on the Russian Far East Coast: Deep-Water and Coastal Observations,* Pure Appl. Geophys., 1–22. doi:10.1007/s00024-013-0727-1.

SONG, Y.T. and T.Y. HOU (2006). *Parametric vertical coordinate formulation for multiscale, Boussinesq, and non-Boussinesq ocean modeling,* Ocean Modelling, *11*(3), 298–332. doi:10.1016/j.ocemod.2005.01.001.

SONG, Y.T., L. FU, V. ZLOTNICKI, C. JI, V. HJORLEIFSDOTTIR, C. SHUM, and Y. YI (2008). *The role of horizontal impulses of the faulting

continental slope in generating the 26 December 2004 tsunami, Ocean Modelling, 20(4), 362–379. doi:10.1016/j.ocemod.2007.10.007.

SONG, Y.T., I. FUKUMORI, C. SHUM, and Y. YI (2012). Merging tsunamis of the 2011 Tohoku-Oki earthquake detected over the open ocean, Geophys. Res. Lett., 39(5). doi:10.1029/2011GL050767.

SPENNEMANN, D.H. (1996). Nontraditional settlement patterns and typhoon hazard on contemporary Majuro atoll, Republic of the Marshall Islands, Environ. Manage., 20, 337–348.

Tang, L., V.V. Titov, E.N. Bernard, Y. Wei, C.D. Chamberlin, J.C. Newman, H.O. MOFJELD, D. ARCAS, M.C. EBLE, and C. MOORE (2012). Direct energy estimation of the 2011 Japan tsunami using deep-ocean pressure measurements, J. Geophys. Res., 117(C8). doi:10.1029/2011JC007635.

TITOV, V. and F. GONZALEZ (1997). Implementation and testing of the Method of Splitting Tsunami (MOST) model, NOAA Tech. Memo. ERL PMEL-112 (PB98-122773), NOAA/Pacific Marine Environmental Laboratory, Seattle, WA, 11 pp.

TORRENCE, C. and G.P. COMPO (1998). A practical guide to wavelet analysis, Bull. Am. Meteorol. Soc., 79, 61–78.

U.S. FISH and WILDLIFE SERVICE (2011). Seabird loses at Midway Atoll Wildlife Refuge greatly exceed early estimates. Press Release, 18th March 2011.

VAN DORN, W. (1984). Some tsunami characteristics deducible from tide records, J. of Phys.Ocean., 14, 353–363.

WILSON, R.I., A.R. ADMIRE, J.C. BORRERO, L.A. DENGLER, M.R. LEGG, P. LYNETT, T.P. McCRINK, K.M. MILLER, A. RITCHIE, and K. STERLING (2012). Observations and impacts from the 2010 Chilean and 2011 Japanese tsunamis in California (USA), Pure Appl. Geophys., 170, 1127–1147. doi:10.1007/s00024-012-0527-z.

WOODROFFE, C.D. (2008). Reef-island topography and the vulnerability of atolls to sea-level rise, Global Planet. Change, 62, 77–96. doi:10.1016/j.gloplacha.2007.11.001.

YAMAZAKI, Y., K.F. CHEUNG, G. PAWLAK, and T. LAY (2012). Surges along the Honolulu coast from the 2011 Tohoku tsunami, Geophys. Res. Lett., 39: L09604. doi:10.1029/2012GL051624.